Performance enhancement of AlGaN/InGaN MQW LED with GaN/InGaN superlattice structure

Article *in* IET Optoelectronics · April 2017

DOI: 10.1049/iet-opt.2016.0141

4 authors:

Rabia Saroosh
National University of Sciences and Technology
1 PUBLICATION **4** CITATIONS
SEE PROFILE

T. Tauqeer
Information Technology University of the Punjab
83 PUBLICATIONS **530** CITATIONS
SEE PROFILE

Sara Afzal
Nassau University Medical Center
28 PUBLICATIONS **56** CITATIONS
SEE PROFILE

Haris Mehmood
Information Technology University of the Punjab
18 PUBLICATIONS **158** CITATIONS
SEE PROFILE

IET Optoelectronics

Research Article

IET Journals
The Institution of Engineering and Technology

Performance enhancement of AlGaN/InGaN MQW LED with GaN/InGaN superlattice structure

ISSN 1751-8768
Received on 31st October 2016
Revised 15th February 2017
Accepted on 17th March 2017
E-First on 3rd July 2017
doi: 10.1049/iet-opt.2016.0141
www.ietdl.org

Rabia Saroosh[1], Tauseef Tauqeer[1,2], Sara Afzal[1], Haris Mehmood[1] ✉

[1]*National University of Sciences and Technology (NUST), Islamabad, Pakistan*
[2]*Information Technology University (ITU), Lahore, Pakistan*
✉ *E-mail: harismehmood560@gmail.com*

Abstract: A gallium nitride (GaN)-based light-emitting diode (LED) structure with 10-period superlattice layers (SLs) of *p*-GaN/*i*-$In_{0.2}Ga_{0.8}N$, inserted between *p*-GaN and 12-period $Al_{0.16}Ga_{0.84}N/In_{0.2}Ga_{0.8}N$ multiple quantum well (MQW) layers, is numerically designed and examined using physical device simulator, SILVACO. The SL structure acts as a confinement layer of holes that serves to mitigate the effects of efficiency droop and leakage current within LED. Consequently, inserting SL structure within epitaxial domain tends to improve the current-spreading capability of the device. The proposed structure is compared with the conventional LED without SL and enhanced LED performance has been demonstrated by the SL-based device. The measured power spectral density and luminous power of the under-investigated device are 8.27 W/cm eV at 433 nm and 3.1 W/cm at 12.32 kA/cm^2, respectively. Correspondingly, the external QE of 25.4% has been determined that is higher than the earlier LED reported with 10-period SL structure of *p*-GaN/*i*-$In_{0.2}Ga_{0.8}N$ and 12-period MQWs of GaN/indium GaN configuration. Moreover, another structure based on 30-period SL was also investigated and the output results exhibited no significant improvement in the efficiency due to thermionic emission and thickness-induced strain factors.

1 Introduction

Solid-state lighting system are gradually replacing the traditional lamp-based system. Such system, based on light-emitting diodes (LEDs), has many advantages over the conventional light-based system such as high-power output, higher conversion efficiency and better luminous performance [1]. Consequently, LEDs have been utilised in a number of lighting applications including sign boards, full-colour displays and traffic light signals [2]. Past few years have seen tremendous progress in the epitaxial growth and chip-size scalable designs of InGaN/GaN multiple quantum well (MQW)-based LEDs. Elevated values of quantum efficiency (QE) can be expected from such devices comprising QWs regions [3–5]; so rather than employing multiple LEDs without QW regions, a single LED based on MQWs layers will suffice for lighting applications. Principally, LEDs can be fabricated either using a lateral structure or in vertical configuration. The vertical structure based on GaN has been anticipated to be the key configuration for achieving enhanced luminous efficacy as well as improved efficiency. Such structure offers several advantages over the lateral structure; primarily amongst them is the contribution by vertical GaN toward mitigating the effects of current-crowding; hence, improving the spreading of current within the device [6]. Coupled with efficient light extraction properties, these vertical LEDs also provide thermally stable operation with good reliability [3, 7]. However, there is a technological limit associated with improving the current-spreading within the device: with GaN LEDs predominantly being utilised for lighting applications, the requirement of high power in such cases increases the effect of current-crowding that becomes significant at correspondingly higher current densities.

To reduce the effect of current-crowding, the uniform spreading of current inside the investigated device is very important. It has been reported that current-crowding could significantly degrade the LED performance at low current densities due to localised heating [8]. Consequently, the high-frequency operation of InGaN-based LEDs is fundamentally limited at higher current densities [9]. Mathematically, the influence of efficiency droop at elevated current densities had been analysed by performing the rate equation analysis on InGaN-based LED [10]. The theoretical efficiencies were then compared with the experimental results and it was deduced that the improvement in current-spreading caused significant enhancement in the efficiency droop [9]. Hence, there must be some alternative means to circumvent the issues originated by efficiency droop. As such, an alternative concept of modulation-doped superlattice layers (SLs) has been introduced for LED device [2]. Placed between the substrate and QW regions, SL layers offer better current-spreading without drastically reducing the efficiency of the device [11]. These modulation-doped layers also act as the current-spreading layers in epitaxial structure and can be used to confine the holes; hence, superior hole injection efficiency can be expected in such devices with the reduced current leakage [2]. The well and barrier regions within SL structure comprise two different materials with different lattice constants that, similarly, diminish the effects of dislocations in the epitaxial structure [12, 13]. Since the energy band gap transition is graded instead of abrupt due to SL configuration, better current spread uniformity can be realised with lower current-crowding effects. SL layers also assist in reducing the thermal generation within the anode and cathode electrodes, thereby leading to increase in the LED QE [11, 14].

In recent years, SL layers of aluminium gallium nitride (AlGaN)/GaN and indium GaN (InGaN)/GaN, both have exhibited good performance on the basis of higher mobility, better current-spreading as well as enhanced quantum efficiency [15, 16]. The electron and hole blocking layers can also be added into the SL structure that can further contribute toward enhancing the output performance of the device [17]. Similar works have been reported on heterostructure LEDs using AlGaN/InGaN layers in SL configurations that have shown promising results [18, 19]. Since, delocalisation of charge carriers from In-rich low-defect density regions is considered to be of the possible reasons for efficiency droop in InGaN-based MQW LEDs [20], this enthuses us with an opportunity to probe into the performance characteristics of the AlGaN/InGaN-based MQW LED with periodic SL structure. Three devices have been simulated using SILVACO with the first device as a conventional AlGaN/InGaN-based MQW LED without any SL structure. The other two MQW devices are based on modulation-doped SL structure of GaN/InGaN layers that have

been integrated between the emitter and MQW regions of the investigated device. About 12 periodic layers of $Al_{0.16}Ga_{0.84}N$/$In_{0.2}Ga_{0.8}N$ material have been incorporated for MQW regions in the simulator. This paper has been divided into two sections. In Section 1, the device configuration for the proposed LED devices with SL structure along with the conventional LED will be discussed along with their energy band diagrams. In Section 2, the proposed LEDs are evaluated and studied, with the corresponding external quantum efficiency (EQE) result compared with the reported work in the literature. Analytical results and plots were extracted through simulation using SILVACO and TONYPLOT software. It has been observed that the proposed structure based on 10-period SL structure exhibited better performance in terms of luminous power output and EQE.

2 Physical device modelling

The industrial simulator SILVACO has been used for the designing and simulation of the proposed LED structure. Specifically, physical device simulation offers better physics insights, realistic predictive performance and scale down the fabrication cost along with the time required to optimise the finalised device structure. While designing on technology computer aided design (TCAD), it is pertinent to include relevant mathematical equations within the simulation framework so as to precisely model the characterisation behaviour of the studied LED device. Detailed schematic representation of the LED devices based on with and without SL structures, followed by brief discussion on mathematical models incorporated for physically modelling the proposed LEDs will be reviewed in detailed.

2.1 Simulation models

Different mathematical models pertaining to semiconductor devices such as LEDs have been established followed by the years of extensive research into the device. Such models have been self-consistently utilised by the simulator in order to yield numerical simulations within the framework of under-investigated device. As such, several LED properties such as transient electrical, luminescence characteristics and power spectral density can be purposefully visualised and plotted with the assistance of SILVACO that uses the Newton method to solve the equations. Various mathematical commands are invoked with the MODELS statement that include strain (CALC.STRAIN), piezoelectric polarisation-induced electric fields (POLARIZATION), multiband K.P model (K.P), Auger recombination (AUGER), Fermi–Dirac statistics model (FERMI), optical recombination model and Lorentz gain-broadening (LORENTZ) models. Poisson's equation, derived from Maxwell's Law, is one of the fundamental equations pertaining to the distribution of electrostatic potential owing to the space charge density, and is expressed according to the following equation [21]:

$$\mathrm{div}(\varepsilon\nabla\psi) = -\rho \tag{1}$$

where is ε the local permittivity, ψ is the electrostatic potential and ρ is the local space charge density. Another equation derived from Maxwell's laws is the continuity equation and it represents the variation in charge carrier densities within the semiconductor device as a result of various physical mechanisms such as transport process, recombination and generation processes. The continuity equation can be mathematically described by the following expression [22]:

$$\frac{\partial n}{\partial t} = \frac{1}{q}\mathrm{div}\,\boldsymbol{J}_n + G_n - R_n \tag{2}$$

$$\frac{\partial p}{\partial t} = -\frac{1}{q}\mathrm{div}\,\boldsymbol{J}_p + G_p - R_p \tag{3}$$

where n and p are the electron and hole concentrations, $\boldsymbol{J}_n$ and $\boldsymbol{J}_p$ are electron and hole current densities vectors, G_n and G_p are electron and hole generation rates, R_n and R_p are the recombination rates for electrons and holes, respectively. The energy band gap of $In_xGa_{1-x}N$ is calculated according to the Vegard's law of band gap [23]

$$E_g(\mathrm{In}_x\mathrm{Ga}_{1-x}\mathrm{N}) = xE_g(\mathrm{In\,N}) + (1-x)E_g(\mathrm{GaN}) - bx(1-x) \tag{4}$$

where x is the In composition in the compound, $E_g(\mathrm{InN}) = 0.65$ eV and b is the bowing parameter ranging from 1 to 6 [23]. For whole In composition x, the value of 1.4 eV is generally used for the bowing parameter [24]. Similarly, the composition dependence of the energy gaps for $Al_xGa_{1-x}N$ is assumed to follow the quadratic form [24]:

$$E_g(\mathrm{Al}_x\mathrm{Ga}_{1-x}\mathrm{N}) = xE_g(\mathrm{AlN}) + (1-x)E_g(\mathrm{GaN}) - bx(1-x) \tag{5}$$

where x is the Al composition, $E_g(\mathrm{AlN}) = 6.2$ eV and $b = 1.3$ eV for AlGaN compound [24]. For modelling of lattice-induced strain and the piezoelectric polarisation-induced effects in LED, the CALC.STRAIN and POLARIZATION parameters are specified in the REGION statement. The piezoelectric polarisation in the InGaN QW can be calculated by using the following relation [25]:

$$P_z(In_x\mathrm{Ga}_{1-x}\mathrm{N}) = 0.148x - 0.0424x(1-x) \tag{6}$$

With x as the In content in QW. Similarly, the K.P model is used for the band parameters as well as the FERMI model. To compute the total radiative recombination rate and include it into continuity equations, SPONTANEOUS model has been used along with CHUANG and LORENTZ. Recombination rate is measured by performing angular average over TE and TM polarisations and integrating over the whole spectrum using Gauss–Laguere quadrature rule [26]

$$R_{sp}(x, y, z) = \int_0^\infty \frac{(2r_{sp}^{\mathrm{TE}}(E) + r_{sp}^{\mathrm{TM}}(E))}{3}\,\mathrm{d}E \tag{7}$$

with r_{sp} (υ = TM or TE) defined as [26]

$$r_{sp}^{\upsilon} = \frac{q^2\pi}{n_{\mathrm{r}}c\varepsilon_0 m_0 w L_z}\sum_{\sigma=U,L}\sum_{n,m} \int \frac{k_t \mathrm{d}k_t}{2\pi}\left|(M_{\mathrm{e}})_{nm}^{\sigma}(k_t)\right|^2 \frac{f_n^c(k_t)(1-f_{\sigma m}^{\upsilon}(k_t))\gamma/\pi}{(E_{\sigma,nm}^{cv}(k_t)-\hbar\omega)^2+\gamma^2} \tag{8}$$

where q is the electron charge magnitude, m_0 is the electron rest mass in free space, c and ε_0 are the velocities of light and permittivity in free space, respectively, n_{r} and L_z are the refractive index and well-width of the QW, and $(\boldsymbol{M}_{\mathrm{e}})_{nm}^{\sigma}$ is the momentum matrix element for transitions between the energy band states, f represents the Fermi–Dirac distribution of electrons and γ is linewidth of the Lorentzian function. Gain-broadening due to intra-band scattering has been introduced with LORENTZ statement which can be described by the following equation [27]:

$$g(E) = \int_{E_{ij}}^\infty g(E')L(E'-E)\mathrm{d}E' \tag{9}$$

where the Lorentzian shape function is given by

$$L(E'-E) = \frac{1}{\pi}\cdot\frac{W_{G0}}{(E'-E)^2 + W_{G0}^2} \tag{10}$$

where $W_{G0} = 0.3$ is the material-related Lorentzian gain-broadening factor used in the simulation and E is the energy centre. All relevant material parameters utilised for simulation of the proposed structure have been tabulated in Table 1.

Table 1 Material parameters values used in SILVACO

Material parameters	$In_{0.2}Ga_{0.8}N$	$Al_{0.16}Ga_{0.84}N$	GaN
electron affinity χ, eV	4.88	4.43	4.4
permittivity ε_r, eV	10.2	8.84	8.9
energy band gap E_g, eV	2.66	3.6	3.42
electron mobility μ_n, cm^2/Vs	450	2000	1000
hole mobility μ_p, cm^2/Vs	90	350	300
effective density of states (DOS) in conduction band N_C, cm^{-3}	1.78×10^{18}	2.25×10^{18}	2.02×10^{18}
effective DOS in valence band N_V, cm^{-3}	8.52×10^{18}	2.04×10^{19}	1.57×10^{19}
hole lifetime τ_p, s	1×10^{-9}	1×10^{-9}	1×10^{-9}
electron lifetime τ_n, s	1×10^{-9}	1×10^{-9}	1×10^{-9}
electron Auger coefficient (AUG_n)	1×10^{-34}	1×10^{-34}	1×10^{-34}
hole Auger coefficient (AUG_p)	1×10^{-34}	1×10^{-34}	1×10^{-34}
radiative recombination rate coefficient (C_{OPT})	1.1×10^{-8}	1.1×10^{-8}	1.1×10^{-8}

2.2 Conventional LED structure

The reference LED device based on conventional configuration is designed in contemplation of analysing the characterisation performance of the device. In this work, the conventional structure of the LED consists of p^+/p/MQW/n/n^+ structure without any periodic SL layers. MQWs comprise charge carrier stopper barrier layers to confine carriers to the active regions in the conduction and valence bands. This MQW structure contains 12-period $Al_{0.16}Ga_{0.84}N/In_{0.2}Ga_{0.8}N$ layers where $Al_{0.16}Ga_{0.84}N$ acts as barrier and $In_{0.2}Ga_{0.8}N$ constitutes well regions in the conventional structure. The thicknesses of 8.5 and 2.5 nm were used in the simulation for wide band gap barrier and narrow gap well, respectively. Generally, *p–n* junction diode is forward biased to inject high concentrations of electrons into the *n*-side and holes into the *p*-side.

Stopper layers confine the charge carriers to the active regions of the device so as to enhance the radiative recombination of electrons and holes within the forbidden band region. This, in turn, gives rise to more output power in terms of luminous intensity. Furthermore, the vertical structure assists in improving the current-spreading and gives a better performance in terms of EQE. The schematic diagram of vertical structure conventional LED device; Device A, along with its energy band diagram, are shown in Figs. 1*a* and *b*, respectively. The epitaxial structure consists of 2 µm *n*-GaN base layer placed at the bottom of the device with the dopant concentration of 1×10^{18} cm^{-3}. Similarly, 0.5 µm *p*-GaN (magnesium doped) emitter layer is inserted at the top of MQWs with dopant values of 4×10^{17} cm^{-3}. To form contact layers with the active regions, the structure was capped on both sides (top and bottom) by heavily doped GaN epilayers. Anode and cathode contacts were placed at the top and bottom of the device, respectively. Relevant material parameters for GaN and $In_{0.2}Ga_{0.8}N$ utilised in the simulation are shown in Table 1.

2.3 LED with periodic SL layers

The proposed LED structure will be discussed in this section. Two GaN-based vertical LED structures incorporating periodic modulation-doped SL layers are designed with the following epitaxial configuration: p^+/p/SL/MQW/n/n^+, where the proposed devices are capped with heavily doped epilayers of GaN. One of such vertical structures comprise 10-period SL structure of *p*-GaN/*i*-$In_{0.2}Ga_{0.8}N$ (2 nm/1 nm), inserted between the MQWs and *p*-GaN regions of the device. An SL structure similar to this was fabricated and characterised by Liu *et al.* [14]. MQW structure is made from the same materials as discussed in the previous section pertaining to Device A. The new proposed device is named as Device B and will be referred to as such in later part of this paper. For further ascertaining the output characteristics of periodic SL-based LEDs, another structure, herein referred to as Device C, is implemented with 30-period SL configuration. The schematic representation of MQW devices based on periodic SL structure is shown in Fig. 2.

The epitaxial structure consists of 2 µm Si-doped *n*-GaN ($n = 1 \times 10^{18}$ cm^{-3}) base layer, 12-period intrinsic $Al_{0.16}Ga_{0.84}N$/*i*-$In_{0.2}Ga_{0.8}N$ (8.5 nm/2.5 nm) MQWs as active layers, followed by 30-period *p*-GaN/*i*-$In_{0.2}Ga_{0.8}N$ (2 nm/1 nm) SL and finally a 0.5 µm thick *p*-GaN ($p = 4 \times 10^{17}$ cm^{-3}). *p*-GaN provides the uniform current-spreading by redistributing the current to the undoped and low-resistive InGaN layers. The corresponding energy band diagram for Devices B and C are shown in Figs. 3*a* and *b*, respectively. The performance characteristics of these two devices with SL are compared with Device A that is devoid of SL structure.

3 Results and discussion

In this section, various results of the numerical solutions demonstrating the device performance characterisations such as band bending phenomena, current–voltage measurements (*I–V*), luminous power output as a function of current and power spectral

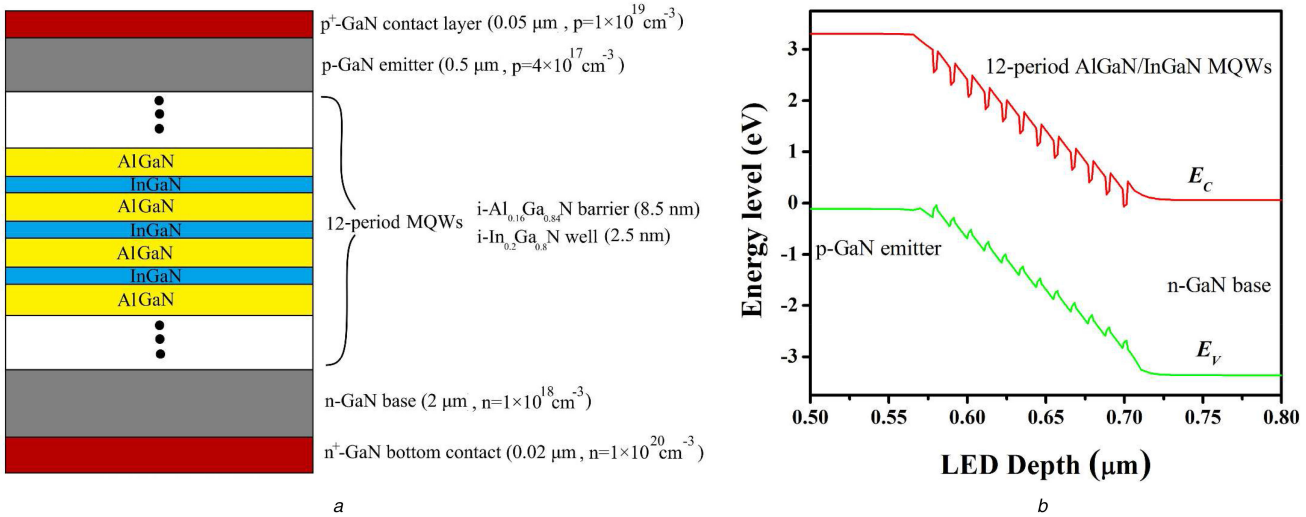

Fig. 1 *SILVACO representation of vertical structure conventional LED device*
(a) Schematic diagram of conventional LED, ***(b)*** Band diagram of LED without SL structure

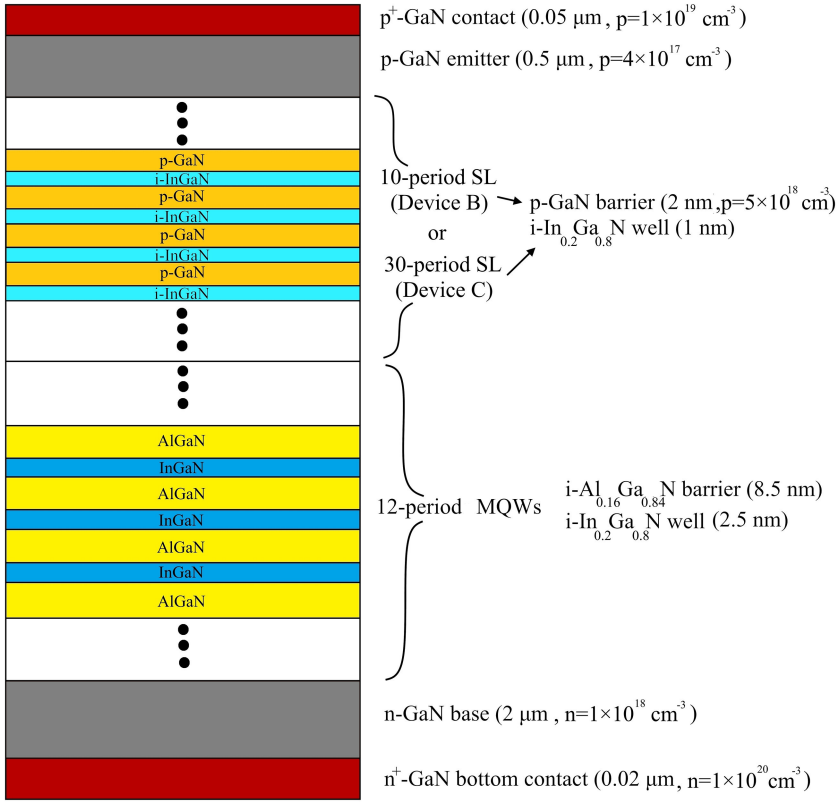

Fig. 2 *Schematic representation of the studied LED with periodic SL structure*

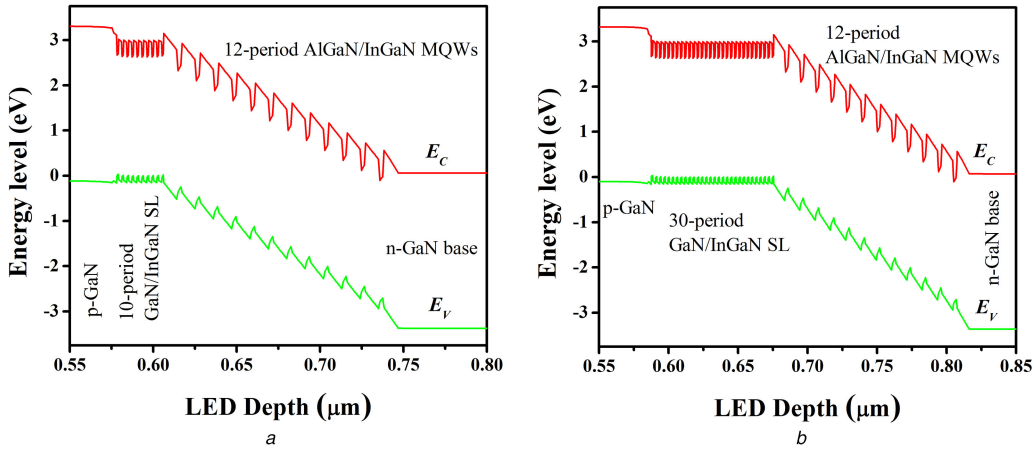

Fig. 3 *Energy band diagram plot for devices based on*
(a) 10-period SL, Device B, ***(b)*** 30-period SL, Device C

density profile are discussed and compared using SILVACO's TONYPLOT graphical module for visualising the solution data files numerically processed by the simulator.

3.1 Band bending and I–V characteristics

As illustrated in energy band diagram plots of the devices with SL configuration, band bending phenomena has been observed owing to the piezoelectric polarisation-induced effects in GaN/InGaN layers. Carriers can easily diffuse along the interface of heterojunctions, and the current-spreading effect can be observed. Prior to injection into GaN barrier, holes are transported laterally in InGaN layers until a higher voltage is applied. The injected carriers then spread substantially widely for devices with SL structure that can be attributed to the band offset between barrier (GaN) and well (InGaN) layers [14]. The result of such current-spreading is manifested in the current density–voltage characteristic plot.

Carrier diffusion and tunnelling are amongst the key mechanisms affecting the charge carrier transport in SL domain [14]. Diffusion process contributes toward current-spreading uniformity, whereas operational voltage can be limited by tunnelling phenomena. When Device B is under forward biased, InGaN layers within SL, which have lower band gap as compared with the GaN, can act as a low-resistive conductive layers with many parallel resistances [14]. The GaN layer which has higher band gap can be treated as the diode connected in series within the periodic SL structure [14]. As the current is fully injected because of the conductive InGaN layers, series diodes prevent the vertical injection of current inside the layers by virtue of higher turn-on voltage. In case of Device A, the carriers do not spread widely because of the absence of SL structure or current-spreading layers; hence, lower current has been observed. As seen from Fig. 4, Device A has low turn-on voltage of 2.7 V, but the amount of current increases gradually. Whereas in case of Device B the turn voltage is a bit high; 3.2 V, but the amount of current grows exponentially. Device C also exhibited almost same performance such as that of Device B despite using larger number of periodic SL layers. The simulated results depict the current density (J_s) measurements of 5.62, 12.32 and 12.02 kA/cm^2 for Devices A, B and C, respectively, at 5 V bias. As discussed, periodic SL layers

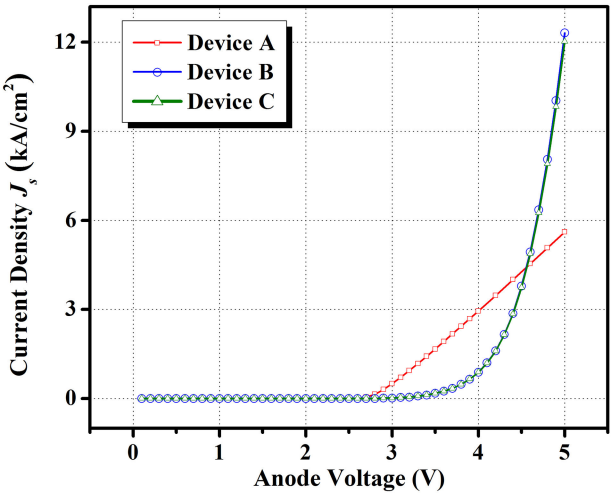

Fig. 4 *J–V characteristics of Devices A, B and C*

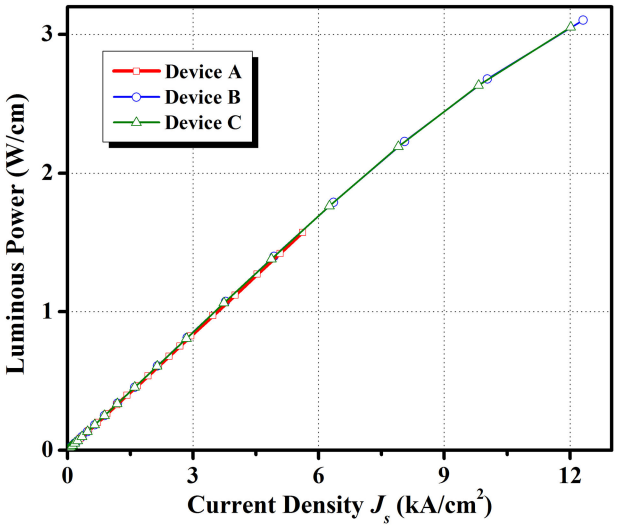

Fig. 5 *Luminous power of LEDs as a function of bias current density*

promote vertical injection of current within the proposed device that consequently leads to the reduction of parasitic resistance and forward voltage. The steep rise in current with respect to voltage for periodic SL-based devices mainly stems from the lower resistance values that can be attributed to the better current-spreading ability induced by the SL structure. These observations are in good agreement with the experimental work reported in the literature [14]. Hence, it has been analytically proved that the electrical *J–V* performance of devices with SL structure is better than the conventional LED (Device A).

3.2 Luminous power

Since all the studied devices are simulated in voltage range of 0–5 V; therefore, it is necessary to determine the current density measurement (J_s) for respective devices in order to analyse the luminous power output. The luminous power of all three devices has been plotted with respect to the current density J_s and shown in Fig. 5. With Device A starting after the turn-on voltage of 2.7 V, its luminous power gradually increases until it reaches a value of 1.54 W/cm at J_s of 5.62 kA/cm^2. For Device B, the luminous power elevates rapidly until it reaches 3.10 W/cm at 12.32 kA/cm^2. Similarly, Device C follows the same trend as Device B, but attains albeit low luminous power of 3.05 W/cm at J_s of 12.02 kA/cm^2. Devices based on periodic SL structure experience high luminous power output and several possible factors may contribute to this improvement such as: (i) improvement in the carrier confinement and current-spreading and (ii) ionisation of electrons at higher bias current leading to enhanced recombination which results in a better performing LED device for optoelectronic applications. However, it can be inferred from Fig. 5 that the power output for Device C decreases by ~2% as compared with Device B that is attributed to the thermionic emission tunnelling at elevated bias current. At low bias, the current is mostly due to recombination in the active region; however, at higher voltage, the current is due to radiative recombination as well as thermionic emission out of the active region. This is so because the quasi-Fermi levels within the active regions shift toward the band and barrier layers become less effective at confining the charge carriers. As a result, carriers leak out from the active regions by thermionic emission phenomena. Another factor contributing to the degraded performance of Device C is due to the strain effects induced by the thickness of SL structure. The InGaN wells in SL structure are under compressive strain due to the lattice mismatch between GaN and InGaN [28]. The cumulative effects of the strain due to 30-period SL is more pronounced when compared with 10-period SL, as a result, degradation in performance was observed for Device C.

3.3 Power spectral density and efficiency measurements

The power spectrum analyses of studied LED devices at fixed bias of 5 V are shown in Fig. 6. Emission spectra for different devices have been obtained by sweeping the bias voltage up to 5 V in TCAD simulator. Here, power spectral density as well as flux spectral density have been extracted through TONYPLOT command in the simulator. The proposed LED Devices B and C numerically achieved high-power output of 8.27 W/cm eV (λ = 433 nm) and 8.22 W/cm eV (λ = 432 nm), respectively. These values are much better than the Device A that delivers 3.07 W/cm eV of spectral power density at 442 nm wavelength. It can be also demonstrated that the increase in height and width of spectral emission is much higher for devices based on periodic SL structure. This can be attributed to the improvement in current-spreading induced by SL structure. The quasi-Fermi levels are deeper in the energy bands and further away from the energy gap for a given amount of applied bias. The carriers which recombine are spread over a larger energy range and thus correspondingly increase in emission width over energy range observed. However, the height and width of spectral emission Device C are comparatively lower than Device B. Key reason for this phenomena is the leakage of electrons out of the active regions by thermionic emission process that prevails at higher bias currents. As discussed, higher bias current restrict the movement of the quasi-Fermi levels further into the band and the width of the emission spectrum is determined by the separation of the electron and hole quasi-Fermi levels. This behaviour has been experimentally observed by Detchprohm *et al.* [29]. Next, Table 2 tabulates the values of radiative recombination and total recombination rate of different devices at 5.62 kA/cm^2 current density in order to find the luminous efficiency of LEDs. The minimum value of current density among the devices has been chosen as a reference point to measure the luminous efficiency. Device A exhibited 79.8% luminous efficiency, whereas Devices B and C numerically demonstrated 82.5 and 81% luminous efficiencies, respectively. The primary reason for Device C's low performance is due to the enhancement in non-radiative recombination rate that can attributed to the leakage of charge carriers from active regions by thermionic emission phenomena as well as strain-induced effects. Similarly, the structures were simulated to find EQE by observing flux spectral density and current measurements at fixed voltage of 5 V.

The reference structure, based on 10-periodic SL and developed by Liu *et al.* [14], has been simulated based on the parameters, models and equations used in our simulation. Our simulations end up with the results which agree with the characterisation results of the fabricated device. Reference LED showed 24.1% EQE at current density of 4.7 kA/cm^2 that is much closer to the experimentally observed EQE of 24.8%. Moreover, lower value of EQE was measured for conventional LED due to the absence of proper current-spreading mechanism. Device B has demonstrated simulated EQE (Table 3) of 25.4% as compared with experimental 24.8% by Liu *et al.* [14]. Nevertheless, Device C recorded low EQE value primarily because of failure to generate more flux

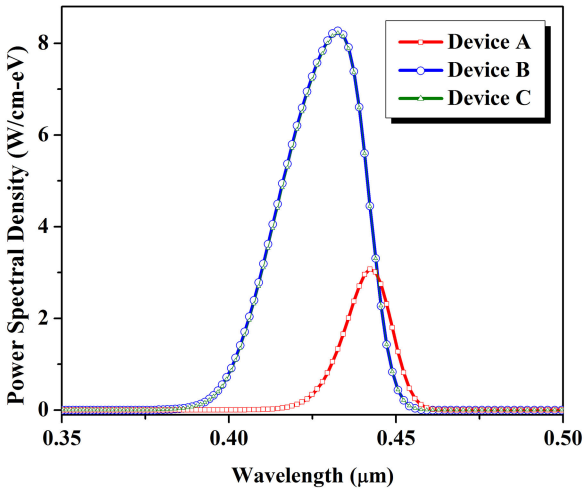

Fig. 6 *Power spectrum of LED devices at 5 V bias*

Table 2 Simulated luminous efficiency measurements at 5.62 kA/cm^2 bias

Device	Radiative rate, cm^3/s (r)	Recombination rate, cm^3/s (T)	Luminous efficiency, % ($\eta_L = r/T$)
Device A	2.80×10^{18}	3.51×10^{18}	79.8
Device B	2.87×10^{18}	3.48×10^{18}	82.5
Device C	2.85×10^{18}	3.52×10^{18}	81.0

Table 3 Simulated EQE measurements at 5 V

Device	Flux spectral density, [s cm eV]$^{-1}$ (Φ)	Bias current, kA/cm^2 (J_s)	EQE, % (EQE = $q\Phi/J_s$)
Device A	6.80×10^{18}	5.62	19.3
Device B	1.95×10^{19}	12.32	25.4
Device C	1.80×10^{19}	12.02	24.0

density despite increasing number of layers in SL structure. Another structure based on 5-period SL layers was simulated with same material parameters and mathematical models employed in our simulation and the results showed luminous efficiency and EQE of 81.7 and 23.2%, respectively. These results validate our hypothesis that MQW-based LED with 10-period SL structure is an optimised and viable candidate to generate higher luminous power output along with enhanced EQE. Increasing the number of SL layers beyond the proposed 10-period SL structure seems to play negligible role in enhancing the power output, hence it is practically feasible to employ the proposed structure for blue LEDs based applications.

4 Conclusion

In this paper, three LED structures based on intrinsic AlGaN/InGaN MQW layers are compared with each other as well as reported structure of InGaN/GaN and analysed in detail. The periodic SL configuration of *i*-InGaN/*p*-GaN (1 nm/2 nm) has been employed for the proposed structure. Lower turn-on voltage has been observed for conventional LED as compared with structures based on SL configuration. Nevertheless, lower current density for Device A has been attributed to the absence of SL structure as the carriers do not spread widely. Vertical injection of charge carriers can be promoted via periodic SL structure that enhances the current-spreading ability of the device. Much larger values of luminous power output can be extracted from the devices based on periodic SL structure because of ionisation of electrons at elevated bias current leading to enhanced recombination. However, luminous power output begin to decrease for Device C at higher level of bias current that can be attributed to the enhancement in non-radiative thermionic emission tunnelling as well as cumulative effects due to thickness-induced strain. Similarly, increase in the height and width of spectral emission is much higher for devices based on periodic SL structure that is correlated with the improvement in current-spreading mechanism. Elevated values of luminous efficiency have been measured for periodic SL-based device, but no significant improvement in performance was observed with 30-period SL layers because of enhancement in non-radiative recombination. The EQE of the proposed Device B has been simulated to be 25.4% which is higher than the already reported work. Moreover, the optimised device based on 10-period SL structure delivered higher luminous power of 8.27 W/cm eV at a wavelength of 433 nm. Another structure based on 5-period SL layers showed luminous efficiency and EQE of 81.7 and 23.2%, respectively. Hence, it has been proved that MQW-based LED with 10-period SL structure is an optimised and viable candidate to generate higher luminous power output along with enhanced EQE for blue LEDs based applications.

5 References

[1] Bender, V.C., Marchesan, T.B., Alonso, J.M.: 'Solid-state lighting: a concise review of the state of the art on LED and OLED modeling', *IEEE Ind. Electron. Mag.*, 2015, **9**, pp. 6–16

[2] Jian-Yong, X., Fang, Z., Guang-Han, F., *et al.*: 'Efficiency enhancement of an InGaN light-emitting diode with a p-AlGaN/GaN superlattice last quantum barrier', *Chin. Phys. B*, 2013, **22**, (11), p. 118504

[3] Laubsch, A., Sabathil, M., Baur, J., *et al.*: 'High-power and high-efficiency InGaN-based light emitters', *IEEE Trans. Electron Devices*, 2010, **57**, (1), pp. 79–87

[4] Crawford, M.H.: 'LEDs for solid-state lighting: performance challenges and recent advances', *IEEE J. Sel. Top. Quantum Electron.*, 2009, **15**, (4), pp. 1028–1040

[5] Yukio, N., Masatsugu, I., Daisuke, S., *et al.*: 'White light emitting diodes with super-high luminous efficacy', *J. Phys. D., Appl. Phys.*, 2010, **43**, (35), p. 354002

[6] Othman, M.F., Ahmad, S., Sa'ad, F.N.A., *et al.*: 'Current crowding effect in lateral and vertical LED configurations: 3D simulation and characterisation'. IEEE Int. Conf. on Control System, Computing and Engineering (ICCSCE), 2012, pp. 530–534

[7] Chu, C.F., Cheng, C.C., Liu, W.H., *et al.*: 'High brightness GaN vertical light-emitting diodes on metal alloy for general lighting application', *Proc. IEEE*, 2010, **98**, (7), pp. 1197–1207

[8] Kim, H., Park, S.-J., Hwang, H.: 'Effects of current spreading on the performance of GaN-based light-emitting diodes', *IEEE Trans. Electron Devices*, 2001, **48**, pp. 1065–1069

[9] Ryu, H.-Y., Shim, J.-I.: 'Effect of current spreading on the efficiency droop of InGaN light-emitting diodes', *Opt. Express*, 2011, **19**, (4), pp. 2886–2894

[10] Ryu, H.-Y., , H.-S.K., Shim, J.-I.: 'Rate equation analysis of efficiency droop in InGaN light-emitting diodes', *Appl. Phys. Lett.*, 2009, **95**, (8), p. 81114

[11] Wen, T.C., Chang, S.J., Lee, C.T., *et al.*: 'Nitride-based LEDs with modulation-doped $Al_{0.12}Ga_{0.88}N$-GaN superlattice structures', *IEEE Trans. Electron Devices*, 2004, **51**, (10), pp. 1743–1746

[12] Nakayama, M., Kubota, K., Kato, H., *et al.*: 'Effects of buffer layers in GaAs–$In_{0.2}Al_{0.8}As$ strained-layer superlattices', *Appl. Phys. Lett.*, 1986, **48**, (4), pp. 281–283

[13] Kawai, T., Yonezu, H., Ogasawara, Y., *et al.*: 'Suppression of threading dislocation generation in highly lattice mismatched heteroepitaxies by strained short-period superlattices', *Appl. Phys. Lett.*, 1993, **63**, (15), pp. 2067–2069

[14] Liu, Y.J., Tsai, T.Y., Yen, C.H., *et al.*: 'Characteristics of a GaN-based light-emitting diode with an inserted p-GaN/i-InGaN Superlattice structure', *IEEE J. Quantum Electron.*, 2010, **46**, (4), pp. 492–498

[15] Shuti, L., Qibao, W., Guanghan, F., *et al.*: 'Influence of a p-InGaN/GaN short-period superlattice on the performance of GaN-based light-emitting diodes', *Semicond. Sci. Technol.*, 2009, **24**, (8), p. 85016

[16] Yan Zhang, Y., An Yin, Y.: 'Performance enhancement of blue light-emitting diodes with a special designed AlGaN/GaN superlattice electron-blocking layer', *Appl. Phys. Lett.*, 2011, **99**, (22), p. 221103

[17] Liu, C., Lu, T., Wu, L., *et al.*: 'Enhanced performance of blue light-emitting diodes with InGaN/GaN Superlattice as hole gathering layer', *IEEE Photonics Technol. Lett.*, 2012, **24**, (14), pp. 1239–1241

[18] Xiong, J.-Y., Xu, Y.-Q., Zheng, S.-W., *et al.*: 'Advantages of GaN based light-emitting diodes with p-AlGaN/InGaN superlattice last quantum barrier', *Opt. Commun.*, 2014, **312**, pp. 85–88

[19] Yu, C.-T., Lai, W.-C., Yen, C.-H., *et al.*: 'Effects of InGaN layer thickness of AlGaN/InGaN superlattice electron blocking layer on the overall efficiency and efficiency droops of GaN-based light emitting diodes', *Opt. Express*, 2014, **22**, (S3), pp. A663–A670

[20] Monemar, B., Sernelius, B.E.: 'Defect related issues in the 'current roll-off' in InGaN based light emitting diodes', *Appl. Phys. Lett.*, 2007, **91**, (18), p. 181103

[21] Streetman, B., Banerjee, S.: '*Solid state electronic devices*' (Prentice-Hall Inc., 2006, 6th edn.)

[22] Sze, S.M., Lee, M.K.: '*Semiconductor devices: physics and technology*' (John Wiley & Sons Ltd., 2012, 3rd edn.)
[23] Hussain, S., Ali, G., Mehmood, H., *et al.*: 'Theoretical studies of InGaN/GaN multiple junction solar cell with enhanced tunneling junction diode', *Adv. Mater. Res.*, 2014, **895**, pp. 535–538
[24] Vurgaftman, I., Meyer, J.R.: 'Band parameters for nitrogen-containing semiconductors', *J. Appl. Phys.*, 2003, **94**, (6), pp. 3675–3696
[25] Arif, R.A., Zhao, H., Ee, Y.-K., *et al.*: 'Radiative efficiency and spontaneous recombination rate of staggered InGaN quantum well LED at 420-510 nm', *Proc. SPIE, Light-Emitting Diodes, Res. Manuf. Appl. XII, 691014*, 2008, **6910**, pp. 691010–691014
[26] Chuang, S.L.: 'Optical gain of strained wurtzite GaN quantum-well lasers', *IEEE J. Quantum Electron.*, 1996, **32**, pp. 1791–1800
[27] Neogi, A., Lee, C.-W., Everitt, H.O., *et al.*: 'Enhancement of spontaneous recombination rate in a quantum well by resonant surface plasmon coupling', *Phys. Rev. B*, 2002, **66**, (15), p. 153305
[28] Kim, C.S., Kim, H.G., Hong, C.-H., *et al.*: 'Effect of compressive strain relaxation in GaN blue light-emitting diodes with variation of n^{+}-GaN thickness on its device performance', *Appl. Phys. Lett.*, 2005, **87**, (1), p. 13502
[29] Detchprohm, T., Hiramatsu, K., Sawaki, N., *et al.*: 'Metalorganic vapor phase epitaxy growth and characteristics of Mg-doped GaN using GaN substrates', *J. Cryst. Growth*, 1994, **145**, (1), pp. 192–196